Wake interactions of two tandem floating offshore wind turbines: CFD analysis using actuator disc model

Abdolrahim Rezaeiha [a, b, *], Daniel Micallef [c]

[a] *KU Leuven, Belgium*
[b] *Eindhoven University of Technology, the Netherlands*
[c] *University of Malta, Malta*

ABSTRACT

Floating offshore wind turbines (FOWTs) have received great attention for deep water wind energy harvesting. So far, research has been focused on a single floating rotor. However, for final deployment of FOWT farms, interactions of multiple FOWTs and potential impacts of the floating motion on power performance and wake of the rotors need to be investigated. In this study, we employ CFD coupled with an Actuator Disc model to analyze interactions of two tandem FOWTs for the scenario, where the upstream rotor is floating with a prescribed surge motion and the downstream rotor is fixed and influenced by the variations in the incoming flow created by the oscillating motion of the surging rotor. We will investigate three different surge amplitudes and analyze the fluctuations in power performance of the two rotors as well as their wake interactions. The results show a light increase in the mean power coefficient of both rotors for the surging case, compared against the case with no surge motion. The standard deviation of the transient C_P of the surging rotor linearly scales with the surge amplitude, while such impact for the downstream rotor is very limited. Surging motion of the upstream rotor is found to enhance flow mixing in the wake, which therefore, accelerates the wake recovery of the downstream rotor. This finding suggests prospects for research into redesigning wind farm layout for FOWTs, aiming for more compact arrangements.

© 2021 The Authors. Published by Elsevier Ltd. This is an open access article under the CC BY license (http://creativecommons.org/licenses/by/4.0/).

1. Introduction

1.1. State of the art and challenges

The increasing interest in Floating Offshore Wind Turbines (FOWTs) has triggered numerous research efforts in various directions including, for instance, floaters, mooring lines, hydrodynamics, aerodynamics, structural fatigue and a further interest in upscaling rotors (see Bento and Fontes [1]). Now, the main challenge that needs to be overcome is the high Levelized Cost of Energy (LCoE) such as mentioned by Bosch et al. [2] and Kausche et al. [3]. Improving blade design and performance remains an important topic to address the LCoE problem [4]. With improved loading predictions, blades can be designed better, and maintenance schedules can be driven by informed guidelines. Despite the good knowledge accumulated in the past twenty years or more for the

fixed rotor situation, the floating rotor exhibits highly complex three-dimensional motions because of the hydro-aerodynamic interactions acting on the whole structure. The resulting wake flows are, therefore, increasingly complex because of phenomena such as blade-vortex interaction, vortex-vortex interactions, blade flow three-dimensionality as well as unsteady airfoil behavior and dynamic stall.

Due to these intrinsic complexities, current research efforts in hydrodynamics and aerodynamics remains mainly uncoupled, with few exceptions such as Wang et al. [5] and Liu et al. [6]. With respect to hydrodynamics, full-body Navier-Stokes simulations have been used to predict loading on both the foundation [7] as well as mooring lines [8]. More simplified methods based on the FAST (Fatigue, Aerodynamics, Structures, and Turbulence) code, developed by National Renewable Energy Laboratory (NREL) [9], have been used for the analysis of these loads by Roald et al. [10]. Chan et al. [11] also developed an approach using fluid-impulse theory for load calculation and implemented a module in FAST. Experimental measurements of hydrodynamic loads have also been carried out by Shin et al. [12]). Apart from information on loads,

Nomenclature

α	Angle of attack [°]
ω	Specific dissipation rate [1/s]
ω_x	Rotor surge frequency [Hz]
Ω	Rotor rotational speed [rad/s]
Φ	Blade azimuth angle [°]
ε_i	Scaling factor
ρ	Air density [kg/m^3]
η	Gaussian function
λ	Rotor tip speed ratio
Δx	Maximum airfoil thickness [m]
Δu_m	Time-averaged axial velocity deficit [m/s]
a	Axial induction factor
a_2	Tangential induction factor
A	Rotor surge amplitude [m]
B	Number of blades
c	Chord length [m]
C_T	Thrust coefficient
C_P	Power coefficient
CoP	Pressure coefficient
D	Rotor diameter [m]
F	Force [N]
k	Turbulence kinetic energy [m^2/s^2]
P	Rotor power [W]
r	Rotor radius at a blade section [m]
R	Rotor radius [m]
S	Source term vector [N/m^3]
t	Time [s]
t_s	Surge period [s]
T	Thrust force [N]

V	Velocity vector at a blade section [m/s]
u	Instantaneous axial velocity [m/s]
u'	Fluctuations of axial velocity [m/s]
u_m	Time-averaged axial velocity [m/s]
u_s	Rotor surge velocity [m/s]
u_{std}	Standard deviation of u' [m/s]v
v	Instantaneous tangential velocity [m/s]
V_{rel}	Flow relative velocity [m/s]
U_∞	Freestream/reference wind velocity [m/s]
x, y	global coordinates (origin at rotor1 center)
x_i	x-coordinate of control volume cell center
x_s	Rotor surge displacement [m]
AD	Actuator Disc
AL	Actuator Line
AEP	Annual Energy Production
BEM	Blade Element Momentum
BET	Blade Element Theory
CRAFT	Coupled Response Analysis of Floating wind Turbine
CFD	Computational Fluid Dynamics
FAST	Fatigue, Aerodynamics, Structures, and Turbulence
FOWT	Floating Offshore Wind Turbine
FVWM	Free Vortex Wake
HAWT	Horizontal Axis Wind turbine
LCoE	Levelized Cost of Energy
LES	Large Eddy Simulation
NREL	National Renewable Energy Laboratory
NVLM	Non-linear Vortex Lattice Method
SST	Shear Stress Transport
TLP	Tension-Leg Platform
VLM	Vortex Lattice Method
URANS	Unsteady Reynolds-Averaged Navier Stokes

better hydrodynamic models allow for a better prediction of the motion of the wind turbine. With an uncoupled aerodynamic approach, such motions have to be prescribed and therefore this information becomes essential in the study of FOWTs. The uncoupled high-fidelity aerodynamic analysis of FOWTs, such as Computational Fluid Dynamics (CFD) simulations, mainly employs such prescribed platform motions obtained from lower-fidelity coupled analysis tools, such as FAST. This uncoupled approach could already be very insightful with respect to elucidating the novel unsteady aerodynamic phenomena associated FOWTs and, thus, could be employed to improve the lower-fidelity models. In addition, these are useful since they provide a quicker alternative to coupled simulations and are able to provide an accurate description of the physics (see Sebastian and Lackner [13]).

FOWTs experience various motions of the platform and they have distinct effects on the wake aerodynamics. Among the motions, the pitching and surging platform motions are identified as the two dominant motions for FOWTs [14], therefore, the majority of the literature have focused on these two motions [15]. The effects of platform pitching motion on rotor power performance and wake were investigated by several authors such as Fang et al. [16], Fu et al. [17], Shen et al. [18], Leble and Barakos [19]. For example, Wen et al. [20] studied the rotor power for different tip speed ratio and reduced frequency and showed that the power variation increases with increasing tip speed ratio and reduced frequency. This is consistent with earlier findings from Sant et al. [21] and Micallef and Sant [22] in independent experimental and numerical campaigns, respectively. Alternative approaches such as the use of vortex lattice methods (VLM) to study the effect of platform pitching was carried out by Jeon et al. [23], where the presence of a

turbulent wake state was also noted under low speed inflow conditions. Lin et al. [24] report full body rotor CFD computations involving both pitching and surging motion to analyze the unsteady aerodynamics of the rotor.

Surging is the other dominant platform motion for FOWTs and has received attention in the literature, and is also the focus of this study. Table A.1, given in Appendix A, provides an overview of earlier studies focused on surge motion of FOWTs. Except very few experimental works such as [21,25], the studies are mainly numerical. Various modeling approaches were successfully validated including Blade Element Momentum (BEM) methods, free vortex wake models (FVW), actuator disc coupled with CFD (CFD-AD), fully-resolved CFD, however, most of the studies are performed using lower-fidelity modeling tools such as FAST, where different floater types, namely spar-buoy, barge, semi-submersible and tension-leg platform (TLP), have been studied. The higher-fidelity modeling approaches such as CFD-AD and fully-resolved CFD have recently become more common to study FOWTs and have been mainly employing platform motions prescribed through the use of FAST [22,26,27].

Some of the main conclusions regarding the impact of the surge motion on the aerodynamic performance of FOWTs are as follows. The experimental work of Sant et al. [21] and the numerical work of Micallef and Sant [22] showed that the amplitude of oscillations in rotor thrust and power due to surge motion grow for higher tip speed ratios. CFD simulations of Tran et al. [28] and Tran and Kim [29] studied a surging rotor at different surge amplitudes A and frequencies ω_x and found that the unsteady aerodynamic loads and the near wake are significantly influenced due to the surge motion and the instantaneous spatial distribution of the tip vortices is

modified. An increase in the amplitude of power and thrust oscillations for higher ω_x and A is also shown. The numerical results of Kopperstad et al. [30] showed a faster wake recovery for a surging rotor due to large oscillations in rotor loads, the resultant unsteadiness in the wake and the instabilities in the shear layer. The recovery rate became faster for higher dominant wave periods. The study suggests that this can be leveraged to design higher power density wind farms. Kyle et al. [31] investigated the formation of the propeller and vortex ring states for surging rotors with low wind speed and high A. Schliffke et al. [32] experimentally analyzed the wake of a porous disc with a prescribed surge motion with different surge amplitudes and frequencies. They study reported insignificant influence of ω_x and A on the mean velocity profiles. In addition, their presented spectral analysis showed the footprint of the surge frequency on the velocity data at 4.6D downstream of the actuator disc.

Wake interactions between wind turbines located at different positions relative to each other is a subject of particular importance in the context of wind farms design. Such interactions of multiple fixed rotors have been studied numerous times in the past for HAWTs (see for instance Refs. [33,34]) as well as vertical axis wind turbines (e.g. Refs. [35—38]). On the contrary, the case of multiple FOWTs and their wake interactions have received little attention. The differing characteristics of such a problem is that if the downstream turbine is located in the wake of the upstream turbine, the inflow of this turbine will exhibit multiple sources of unsteadiness including that due to the relative motion of the rotor and also due to dynamic wake condition of the upstream turbine. Rockel et al. [39] proposed that turbine spacings for FOWTs might not necessarily be the same as fixed foundation wind turbines. A recent study by Rezaeiha and Micallef [40] employed CFD-AD to investigate two tandem floating rotors with a distance of 3 rotor diameters, where the upstream rotor is oscillating with a prescribed surge motion and the downstream rotor is under its influence. The analysis showed significant impact of the upstream rotor surge motion on the fluctuations of the power performance of the downstream rotor. The present work is designed in the same direction to look deeper into aerodynamic interactions of two tandem floating offshore wind turbines and to further analyze the fluctuations in the power performance of the tandem turbines for different surge amplitudes.

1.2. Novelty and objectives

The aim of this work is to develop a fundamental insight on the wake interactions of floating offshore wind turbines and revealing its consequences on the power performance of the individual turbines and opportunities for optimizing the layout design of floating offshore wind farms. This goal is to be achieved by numerically investigating two tandem (in-line) rotors, for a case where the upstream rotor is exhibiting surge motion while the downstream rotor is fixed. This analysis will shed light on the fundamental physics of the problem and will pave the way for more detailed investigations. To have a broader picture of the basic physical behavior of such rotors, the analysis will be carried out for various surge amplitudes. The objectives of the work are as follows:

- Understanding the impact of the floating surge motion, with different surge amplitudes, on the time-averaged and transient power performance of the two tandem rotors: the level of variation in the mean and standard deviation of thrust and power coefficients for the surging rotor and its downstream rotor will be quantified and correlations between their observed trends will be analyzed.

- Evaluating the frequency effects of the floating surge motion on the rotors power performance: spectral analysis of the transient signals of the surging rotor and the downstream rotor will be performed to identify the contributing frequencies.
- Elucidating the influence of the floating surge motion and surge amplitude on the wake recovery of the rotors: the mean and standard deviation of velocity and pressure in the rotor wakes will be investigated for the fixed rotor case and the case with surging rotors (with different surge amplitudes) in order to study how surge motion affects wake recovery (and amplitude) and to see whether the requirements for the layout design of FOWTs could be different than the fixed rotors.

As shown in Table A.1, given in Appendix A, previous literature of aerodynamic studies of FOWTs is limited to single rotor cases and wake interactions of multi-rotor FOWTs has not yet been investigated. In that sense, this work is one of the first to initiate this research line.

A preliminary set of results was presented in TORQUE2020 conference [40], and this work contains the complete set of results for multiple rotor surge amplitudes with extensive analysis.

Note that a distance of 3 rotor diameters is selected between the two tandem in-line rotors in this study. This distance represents the closet distance that could be considered for a compact rotor arrangement, where the rotors are still safely located outside in the near wake, typically extending up to 1—2 rotor diameter downstream. In addition, for this comparatively small rotor distance, in comparison to more popular distances of 5 or 7 rotor diameter, any possible interactions are amplified and would resemble a better case for a first study and a possible worst case scenario. Indeed, for larger rotor distance, the reported observations due to rotors wake interactions could be diminished.

1.3. Paper structure

The paper will first introduce the methodology used for the numerical modeling of the two tandem floating rotors in Sec. 2. This will include description of the turbine characteristics, the CFD setup and the details of the actuator disc model coupled in CFD. In addition, the test matrix will also be presented in this section. Sec. 3 will elaborate on the power performance of the floating rotors and the wake interactions will be discussed in Sec. 4. Finally, discussion and conclusions will be given in Sec. 5-6.

2. Methodology

2.1. Overview

CFD simulations, coupled with an actuator disc (AD) model, is employed to model two tandem floating offshore wind turbines. CFD modeling coupled with AD (referred to as CFD-AD) is an established modeling approach in wind turbine aerodynamic research, which has also been adopted for floating wind turbines by Micallef and Sant [22] and de Vaal et al. [27]. In this approach, the rotor loading is calculated using the Blade Element Theory (BET) and introduced in the Navier-Stokes equations as a source term in the axial and tangential momentum equations.

In this study, a floating rotor with a prescribed sinusoidal surging motion is positioned upstream of a fixed rotor. The distance between the two in-line rotors is 3 rotor diameters, where such a distance is a lower bound to what would be expected and therefore, we wanted to study this situation as a starting point. In addition, the distance results in more amplified wake interactions between the two rotors, which helps realizing the objectives of this study. Assigning prescribed surging motion for FOWTs in CFD, is a

common decoupled approach in the literature, where the characteristics of the surge motion are typically obtained using lower-fidelity coupled modeling approaches, such as FAST. Note that in the case where the aerodynamics is decoupled from the hydrodynamics, there is also the problem of prescribing platform motions of turbines in the wind farm context. While in the single rotor case, the platform motions can be described from lower fidelity coupled simulations, two rotor cases cannot be modeled with simplified approaches. Effectively this means that the platform motion of the downstream turbine will be influenced by the behavior of the upstream rotor.

Therefore in the present study, as it is aimed to provide further understanding on the influence of a FOWT in surge motion on the power performance of a downstream rotor and their wake interactions, the downstream rotor is modeled as a fixed rotor. This simplification enables us to follow the objectives. In addition, introducing the surge motion for the downstream rotor, although happens due to a combination of hydrodynamic loads and the wake interactions, further complicates the modeling as well as the analysis. A schematic of the simulation setup is given in Fig. 1.

2.2. Turbine characteristics

The employed rotor in the modeling is the National Renewable Energy Laboratory (NREL) 5 MW reference wind turbine with geometrical and operational characteristics given in Table 1. The employed airfoils in the rotor are shown in Fig. 1 and further details are available in the original document by NREL [41].

NREL 5 MW is the most used rotor in FOWT literature allowing for cross-comparison of the results, see Table A.1 in Appendix A. In addition, the choice is made to avoid the need for additional solution verification study, so that the authors can confidently rely on their previously performed verification analysis given in Micallef and Sant [22]. Nevertheless, the derived conclusions regarding the

Table 1
Summary of NREL-5MW design characteristics.

Parameter	
Wind regime	IEC Class 1A
Rotor orientation	Upwind
Control	Variable speed, pitch-regulated, yaw controlled
Number of blades	3
Rotor diameter	126 m
Hub diameter and height	3 and 90 m
Cut-in/-out wind speed	4/25 ms^{-1}
Rated wind speed	11.4 m/s
Rated rotor speed	1.267 rad/s
Rated power	5.0 MW
Rated tip speed	90 m/s

wake interactions of the FOWTs will still be relevant for upscaled rotors such as the 10 MW + rotors.

2.3. CFD: settings, verification and validation

CFD simulations are based on solving the axisymmetric incompressible unsteady Reynolds-Averaged Navier-Stokes (URANS) equations using the commercial CFD solver ANSYS v16.1 [42]. The size of the computational domain is $56R \times 20R$. The upstream rotor (rotor 1) is positioned $10R$ from the domain inlet and the downstream rotor (rotor 2) is positioned $40R$ from the domain outlet. The distance between the two tandem rotors is $3D$. The blockage ratio, defined as the rotor radius over the domain width, is 5%, which is in agreement with guidelines for CFD simulations of wind turbines, e.g. Refs. [43,44]. The computational grid is fully structured with local refinement in the region where the rotors are located and downstream in their wake. The grid size along the rotor span is 1 m, uniformly distributed from root to tip, resulting in 63 cells along the radius. The total cell count is 75,152. Fig. 2
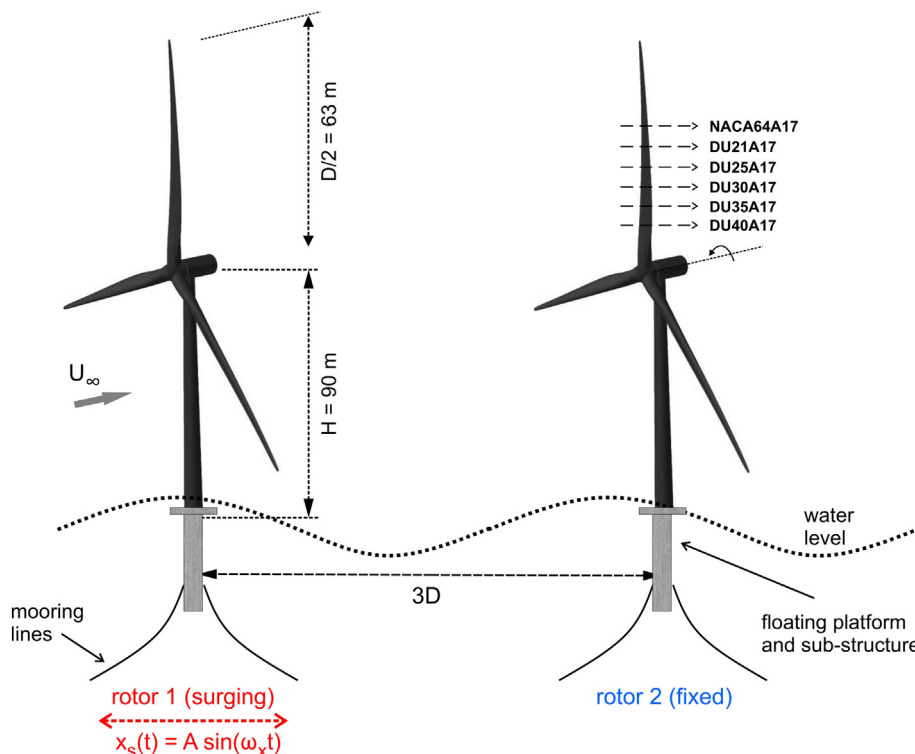

Fig. 1. Case under investigation: two in-line floating NREL 5 MW rotors.

illustrates the computational domain and grid.

Turbulence is modeled using the two-equation SST $k - \omega$ turbulence model. Among the commonly-used RANS turbulence models, the SST model has shown reasonable agreement with experimental data [45] as we as more complex turbulence modeling approaches [46] for wind turbine cases, where complex unsteady aerodynamics plays an important role, which is also the case for FOWTs.

The boundary conditions are as follows: uniform velocity inlet with a total turbulence intensity of 5%, zero static gauge pressure outlet, symmetry in the top and axis in the bottom. The equations are solved using second-order discretization in space and time with SIMPLE pressure-velocity coupling scheme. The time-step for the transient simulations is 0.04 s, resulting in 225 time steps per surge periods. The number of iterations per time step is 20. This ensures that in every time step the scaled residuals drop below 10^{-5}.

The transient simulations are initialized using the steady RANS solution for the fixed rotors. An initialization phase of 15 full surge periods is considered to reach statistically steady state condition. This ensures that the thrust and power coefficients of rotor 1 (averaged over one surge period) have less than 0.5% cycle-to-cycle variations. In addition, the average absolute deviation of the rotor torque between revolution 16 and 17 are less than 0.5%. The presented results correspond to 100 full surge periods from period 15 to 115.

The impact of turbines in CFD modeling is included by introducing the aerodynamic loading using source terms in axial and tangential momentum equations, where the loading is calculated using the actuator disc model described in Sec. 2.4.

The present CFD-AD model is already verified and validated, where details of the solution verification analysis, including grid sensitivity study, and validation study are presented in our previous published work [22,47], and for brevity are not repeated here. As an example, a comparison of results of the present CFD-AD model for power and thrust coefficients of a fixed rotor against blade-resolved CFD and experimental data has been performed and good agreement was observed, see Ref. [47]. A time-step sensitivity analysis is also performed, and the present results are compared with the values calculated using a two times finer time step. Fig. 3 shows the
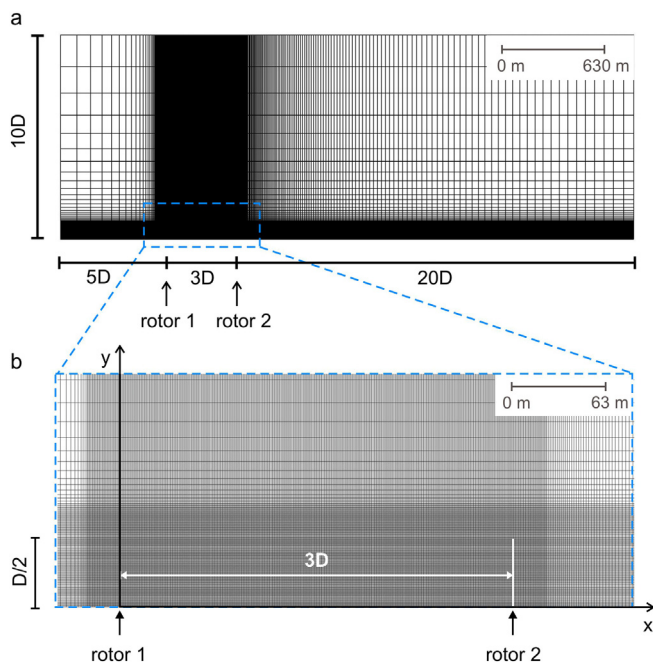
fluctuations in the torque and thrust force of the surging rotor calculated using different time steps, where negligible difference is observed.

2.4. Actuator disc model

Blade Element Theory (BET) is used to establish the loads acting on the actuator discs for the upstream and downstream rotors. Given that the case considered is for two in-line rotors, the situation may be fully axisymmetric given that only surge motions are being considered. The relative flow angle will vary with time in a transient manner and will lead to a dynamic behavior. The velocity diagrams for both rotors are shown in Fig. 4. The blue vectors represent the rotor velocities while surging upstream while the red vectors indicate the aerodynamic velocities. Note that incoming flow velocity, U_∞, for rotor 2 is typically significantly lower than rotor 1 due to being in the wake.

The resulting relative flow velocity V_{rel} and angle of attack α are used to find the lift and drag forces from the 2D polars. It must be emphasized that 2D static data is used. The thrust and torque can then be resolved on a radial element. Tip and root losses are corrected using a Prandtl correction [48]. These forces are input as momentum source terms (in the axial and tangential directions). The details of the method are described in previous works [22,27], thus, not repeated here.

The rotor surge motions, surge position x_s and velocity u_s, are input as prescribed sinusoidal motions with given amplitudes A and frequencies ω_x, where t denotes the time.

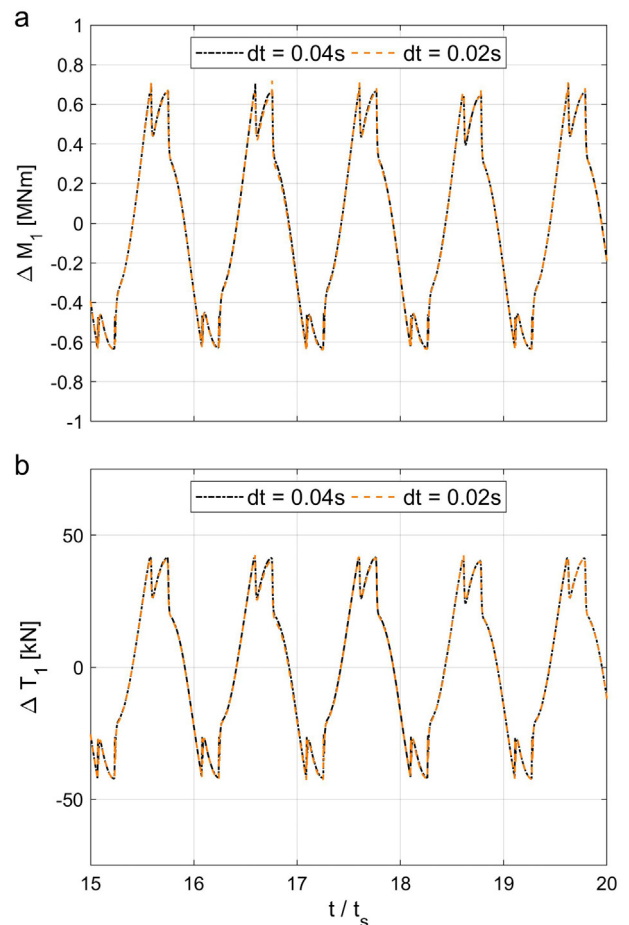**Fig. 2.** CFD simulations: computational domain and grid.

Fig. 3. Time-step sensitivity analysis: fluctuations in the torque and thrust force of the surging rotor calculated using different time steps.
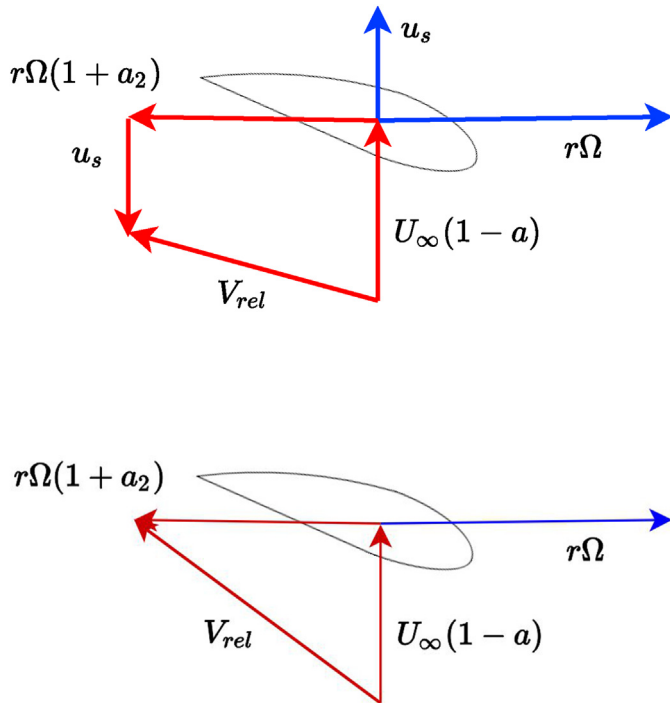
Fig. 4. Velocity diagram for a blade section of the upstream surging rotor (top) and the downstream fixed rotor (bottom). Note that U_∞ for rotor 2 is typically significantly lower than rotor 1 due to being located in the wake. The symbols, r, a, a_2, U_∞, u_s, V_{rel}, Ω denote the radial position along the blade, the axial and tangential induction factors, incoming flow velocity, rotor surge velocity, flow relative velocity, and rotor rotational speed, respectively.

$$x_s(t) = A\sin\omega_x t \tag{1}$$

$$u_s(t) = A\omega_x \cos\omega_x t \tag{2}$$

Predicted forces are blurred using a Gaussian function, η, to minimize issues of singularities which can destabilize the code. This is given by

$$\eta = \frac{1}{\varepsilon\sqrt{\pi}}\exp\left\{\left(\frac{-x_i^2}{\varepsilon}\right)\right\} \tag{3}$$

Where

$$\varepsilon = \varepsilon_i \Delta x \tag{4}$$

ε_i is a scaling factor that should be in the range $1 \leq \varepsilon_i \leq 2$ based on de Vaal et al. [27]. Micallef and Sant [22] also showed that 2.5 is a reasonable choice. Δx is an estimate of the maximum airfoil thickness of the rotor and x_i is the cell center axial coordinate.

The source term vector (S) is found by convoluting the force **F**, blurred using the described blurring function, per unit volume of each annular element ΔV. Note that ΔV is the volume of each annular element given by $2\pi r \Delta r \Delta x$.

$$S = \frac{\int_{-\infty}^{\infty} \mathbf{F}^* \eta dx}{\Delta V} \tag{5}$$

The principal assumption used in the model is that the platform motions of the turbine is prescribed using results from previous work (see Micallef and Sant [22]) which are based on calculations performed in FAST [49]. The platform motions of the downstream turbine will not be identical to that of the upstream turbine due to the wake interference and hydrodynamic effects which will alter system dynamics. Therefore, rotor 2 is kept fixed. With this approach, the simulation complexity is limited but focused on the analysis of the aerodynamics. Also, as rotor 2 for this study is kept fixed, there are no aero-hydrodynamics motions. This justifies the suitability of the methodology. The overall simulation approach is given in the flowchart of Fig. 5.

The choice of the AD model coupled with CFD in the present study is made because the model has been extensively shown to produce reliable results, especially in studies on wake interactions of wind turbine, see for example de Vaal et al. [27], Micallef and Sant [22], Kopperstad et al. [30]. Indeed, blade-resolved CFD would be ideal, however, the complexity and computational cost of multi-rotor simulations of FOWTs would make it hardly affordable for parametric studies. In addition, in this work we are not focused on analyzing local blade physics, therefore, the use of blade-resolved CFD simulations is not justified for the gross quantities such as thrust and power coefficients.

2.5. Test matrix

In the present study, rotor 1 is oscillating with three different surge amplitudes, while rotor 2 is fixed. The test matrix, given in Table 2, provides the details of the surge motion for rotor 1 and the rotor settings for both rotors. Fig. 6 shows the rotor position and velocity for rotor 1 oscillating with different surge amplitudes. Note that as the surge frequency is constant, higher surge amplitude means higher rotor surge speed. The distance between the two rotors is 3 rotor diameter for all cases.

The reference wind speed $U_\infty = 11.4$ m/s is the value at the upstream turbine incidence (x = 0) for the fixed rotor case, also employed in BET calculations to calculate the relative velocity and the angle of attack for rotor 1, and is equal to the NREL 5 MW rated wind speed. The reference wind speed employed in BET calculations for rotor 2 is 5.5 m/s, which corresponds to the mean value at rotor 2 incidence (x = 3D), that is comparatively lower due to the wake of rotor 1, see Sec. 4. Therefore, rotor 2 is not operating at rated condition and has a rotor speed of 0.84 rad/s, see Ref. [41] and Table 2.

3. Power performance

The power performance of the upstream and downstream rotors are discussed in two sub-sections, where in Sec. 3.1 the time-averaged values are discussed and compared against a case with no surge motion. This helps to elucidate to what extent the rotors mean performance is influenced by the surge motion and what would be the difference in predictions if one simplifies the simulation of the surging rotors with fixed one. Sec. 3.2 discusses the transient time-series of the turbines power performance to look more into the unsteady effects due to the surge motion.

3.1. Time-averaged values

The time-averaged power and thrust coefficients (over 100 surge periods) of both upstream and downstream rotors are found to be negligibly affected by the surge motion and the values are insignificantly different than the fixed rotors with no motion. The C_P values marginally increase by 1.2% and 4.2% for the upstream and downstream rotors, for the highest surge amplitude of 3.06 m. The ratio of the C_{P2}/C_{P1} increases from 0.284 for the case with no surge motion to 0.292 for the highest value of A.

The C_T values for rotor 1 marginally decreases by 0.5% for the highest surge amplitude of 3.06 m. The change in the C_T value of
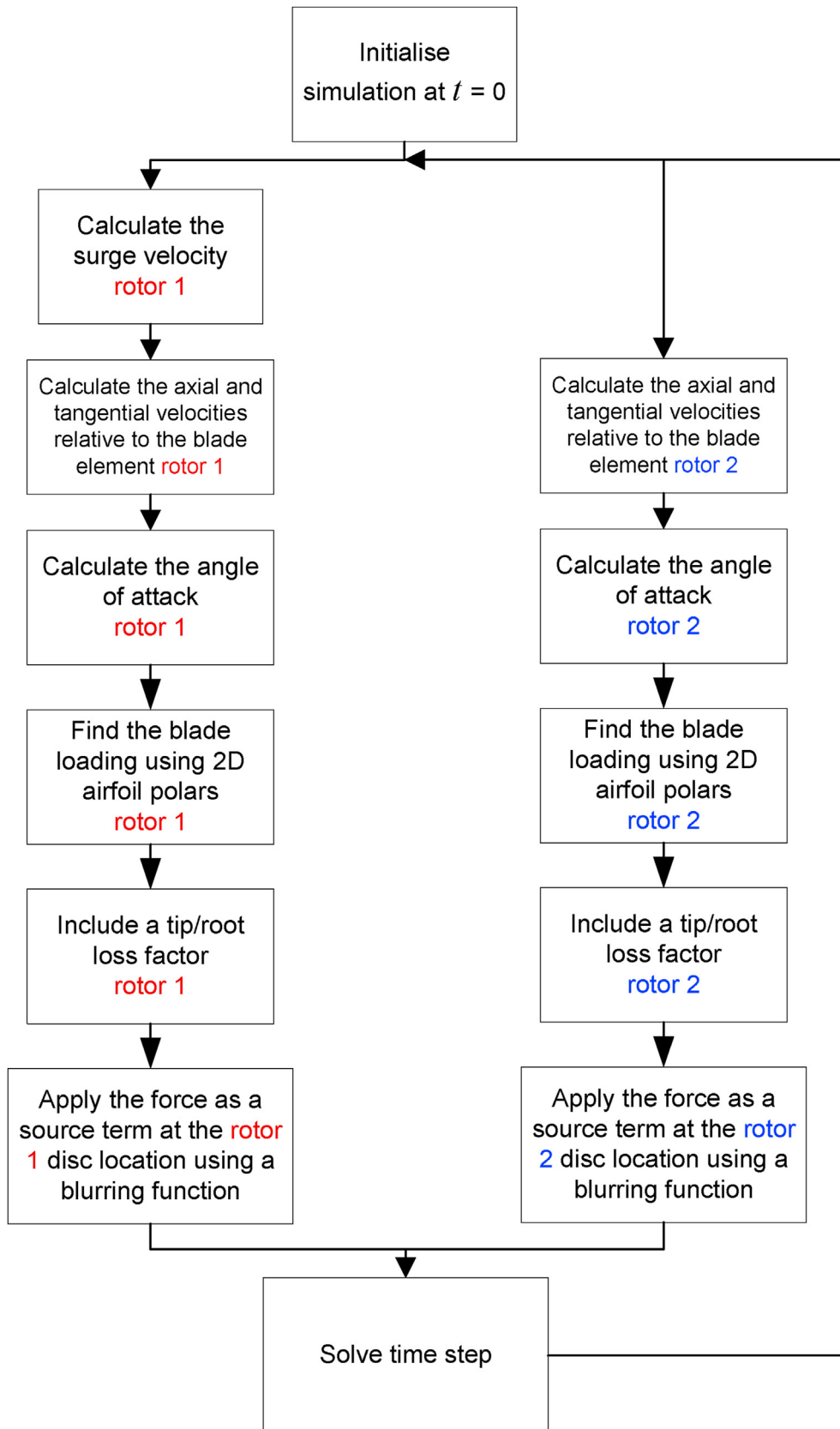
Fig. 5. Overall methodology of the calculation process of the two rotor actuator disc simulations.

Table 2
Platform surge motion characteristics and the rotors settings. Note that the values of A, t_s, and ω_x describe the surge motion amplitude, period, and frequency of rotor 1. The symbols U_∞, λ and Ω denote the incoming flow velocity, tip speed ratio and the rotor rotational speed and the subscripts correspond to the rotor 1 and 2.

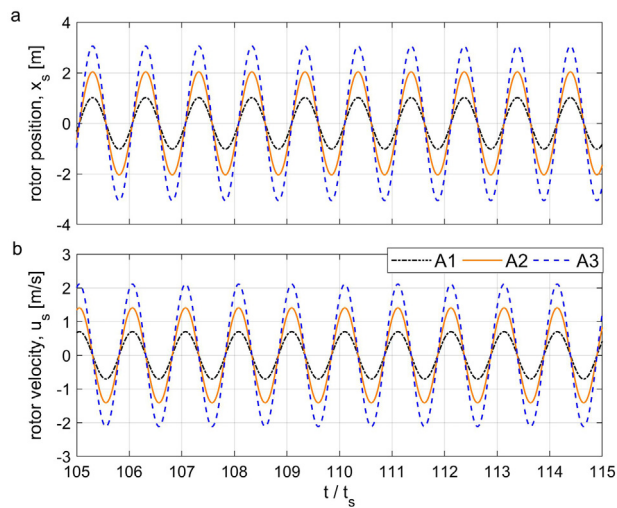|	A [m]	t_s [s]	ω_x [Hz]	U_∞ [m/s]	λ_1	λ_2	Ω_1 in rad/s (in Hz)	Ω_2 in rad/s (in Hz)
A1	1.02							
A2	2.04	9.00	0.11	11.40	7.00	9.62	1.267 (0.2)	0.84 (0.13)
A3	3.06							

Fig. 6. Surge position and velocity for rotor 1 with different surge amplitudes.

rotor 2 and the ratio of the $C_{T,2}/C_{T,1}$ due to the surge motion is negligible.

The fact that the mean power and thrust coefficients of the upstream surging rotor and its downstream rotor are comparable to the case of fixed rotors and insignificantly influenced by the rotor surge motion, is an important finding as it implies that for studies where the focus is on the mean values, for instance when estimating annual energy production (AEP), the fixed rotor coefficients could be a representative indication. Note that in the present study, the employed actuator disc model uses the static airfoil data and this neglects the loads hysteresis due to the excursions of the angle of attack experienced by the blades of the surging rotor and the downstream rotor.

Fig. 7 shows the spanwise distribution of the time-averaged angle of attack α, tangential, F_t, and normal loads, F_n, for the two rotors for the case with no surge motion and the cases with three different surge amplitudes. Overall, the spanwise distribution of the angle of attack and the normal and tangential loads for all cases are comparable, though some differences are also observed. For rotor 1, on the one hand, the tangential loads in the inner blade section, $r/R < 0.36$, are slightly reduced due to the surge motion. This reduction is negligible for the smallest surge amplitude of 1.02 m, however, by increasing the surge amplitude, the reduction grows both in magnitude and the spanwise extent towards the tip. On the other hand, in the outer blade section, $r/R > 0.6$, the tangential loads are increased due to the surge motion and the increment grows for higher surge amplitudes. For rotor 2, the tangential loads experience some increment due to the surge motion in both the inner ($r/R < 0.42$) and outer ($r/R > 0.8$) blade sections. As mentioned before, the integral impact of the surge motion slightly enhances the C_P of both upstream and downstream rotors.

The normal loads for both upstream and downstream rotors are less noticeably affected by the surge motion. This is specially the
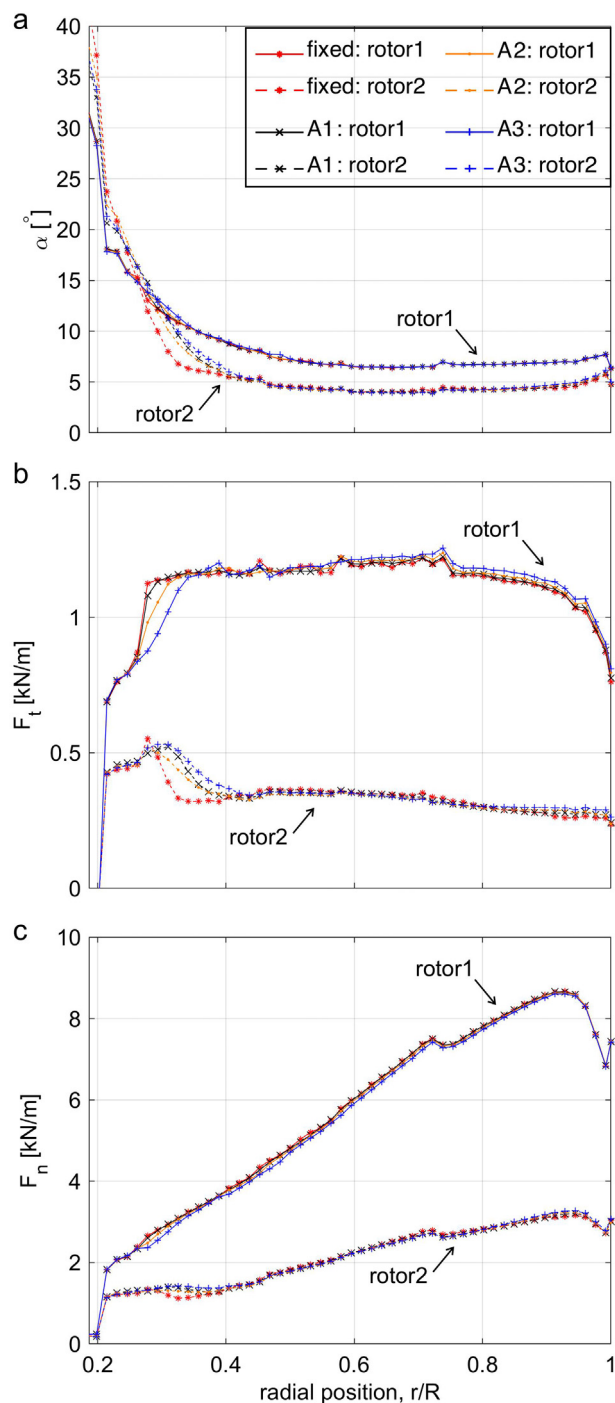

Fig. 7. Spanwise distribution of the time-averaged angle of attack, tangential and normal loads (F_t and F_n) for the upstream and downstream rotors for the case with no surge motion and the cases with three different surge amplitudes.

case for rotor 2. For rotor 1, the normal loads are slightly reduced by the surge motion and this is also in line with the trend observed for C_T. Increasing the surge amplitude has negligible impact.

3.2. Transient data

Fig. 8 shows the fluctuations in the torque and the normalized power coefficient of the oscillating upstream rotor (rotor 1) and the fixed downstream rotor (rotor 2). Rotor 1 is surging with three different amplitudes, given in Table 2. Fig. 9 shows the fluctuations in the thrust force and the normalized thrust coefficient for the same cases. Note that the C_P and C_T values are normalized with the time-averaged value of rotor 1 for the specific surge amplitude. The plots show 10 and 20 full surge periods for rotor 1 and 2 respectively, where the longer frame for rotor 2 is to better visualize the lower frequency harmonics. Note that, as mentioned earlier, for all studied cases rotor 2 is fixed and surging motion is only imposed on rotor 1. The signals are in 180° phase lag with the rotor surge speed depicted in Fig. 6. This means that, as evident, rotor 1 experiences the highest torque and thrust force while surging backward with maximum surge speed, that is due to the comparatively higher relative streamwise velocity, see the velocity diagram in Fig. 4.

Fig. 10 illustrates the spatiotemporal contour plots of the angle of attack, tangential and normal loads (per unit span) for the upstream and downstream rotors. Based on Figs. 8–10, the following observations are made. In general, the transient angle of attack and aerodynamic loads for the case of surging rotor and its downstream turbine, are significantly different than the case of fixed rotors, regardless of the surge amplitude.

The torque, thrust force, C_P and C_T of the upstream (surging) rotor are oscillating with a quasi-sinusoidal motion, dominated by the periodic surge motion of the platform. The results show that the peak-to-peak variations of the oscillating signals scale up with the same factor as the surge amplitude. This is in line with previous findings in the literature [22,27].

The standard deviation of the transient C_P (σ_{C_P}) of rotor 1 with the smallest surge amplitude of 1.02 m is 0.048, that is 8.4% of the respective mean C_P value. By scaling up A to 2.04 m and 3.06 m, σ_{C_P} of rotor 1 proportionally scales up almost with the same factor to 0.094 and 0.139, i.e. 16.5% and 24.1% of the respective mean C_P values.

The standard deviation of the transient C_T (σ_{C_T}) of rotor 1 with the smallest surge amplitude of 1.02 m is 0.027, that is 3.8% of the respective mean C_T value. By scaling up A to 2.04 m and 3.06 m, σ_{C_T} of rotor 1 proportionally scales up almost with the same factor to 0.053 and 0.079, i.e. 7.4% and 11.1% of the respective mean C_T values.

The standard deviation of the fluctuations in torque (σ_M) for rotor 1 with the smallest surge amplitude of 1.02 m is 0.43 MNm. By scaling up A to 2.04 m and 3.06 m, σ_M grows to 0.84 MNm and 1.24 MNm, respectively. The standard deviation of the fluctuations in thrust force (σ_T) for rotor 1 with the smallest surge amplitude of 1.02 m is 26.82 kN. By scaling up A to 2.04 m and 3.06 m, σ_T grows to 52.68 kN and 78.28 kN, respectively. Table 3 lists the mean and standard deviation of the power performance parameters for the discussed cases.

In contrast to rotor 1, the transient torque, thrust force, C_P and C_T time-series of rotor 2 are quite complex signals with several harmonics involved, other than only the main harmonics of the surge motion. For example, a low-frequency period is also observed in the signals of rotor 2, which is absent in the corresponding signals of rotor 1. The complexity is due to the interactions of rotor 2 with the wake of the upstream one. Frequency analysis is presented later in this section.

An important finding is that the overall trend of the oscillating signals is almost invariant to the surge amplitude, although limited differences in the peak values and the standard deviation are observed. The σ_{C_P} of rotor 2 with the smallest surge amplitude of 1.02 m is 0.022, that is 13.6% of the respective mean C_P value. By scaling up A to 2.04 m and 3.06 m, σ_{C_P} of rotor 2 marginally grows to 0.026 and 0.029, i.e. 15.9% and 17.2% of the respective mean C_P values. This means that doubling and tripling the surge amplitude, increases σ_{C_P} by only 15.7% and 29.1%. The σ_{C_T} of rotor 2 with the smallest surge amplitude of 1.02 m is 0.017, that is 6.0% of the respective mean C_T value. By scaling up A to 2.04 m and 3.06 m, σ_{C_T}
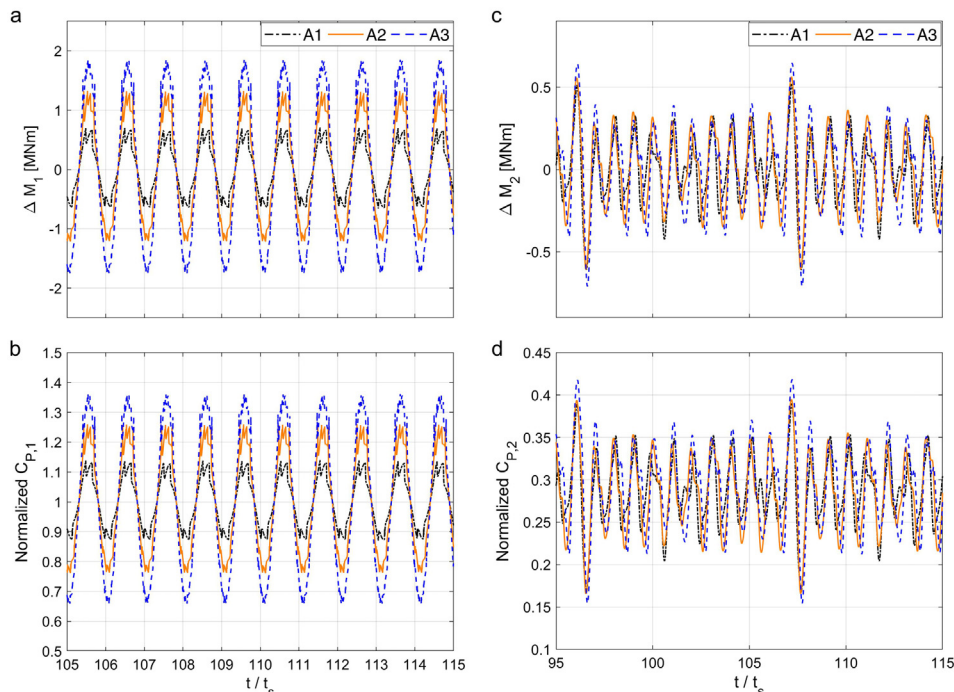

Fig. 8. Fluctuations in the torque and the normalized power coefficient of the oscillating upstream rotor (surging with three different amplitudes) and the fixed downstream rotor.
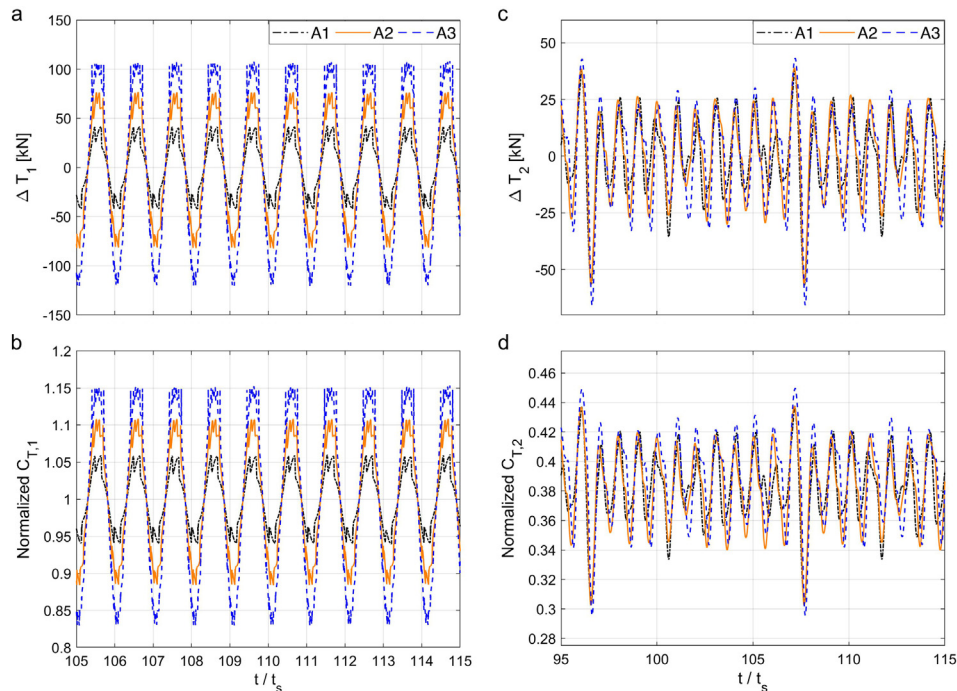
Fig. 9. Fluctuations in the thrust force and the normalized thrust coefficient of the oscillating upstream rotor (surging with three different amplitudes) and the fixed downstream rotor.

of rotor 2 marginally grows to 0.019 and 0.021, i.e. 6.8% and 7.4% of the respective mean C_P values. This means that doubling and tripling the surge amplitude, increases σ_{C_T} by only 12.1% and 24.8%.

Regarding the torque and thrust force of rotor 2, due to the substantial growth in the standard deviation of the signals of rotor 1 due to the increase in A, the ratio between the σ_T and σ_M of rotor 2 to the one of rotor 1 decreases as A increases. By increasing A from 1.20 m to 2.04 m and 3.06 m, the ratio of σ_T of rotor 2 over rotor 1, decreases from 61.2% to 34.8% and 26.1%, respectively. The reduction in σ_M for the same A values is from 46.8% to 27.5% and 20.8%. As rotor 2 is fixed, therefore, the fluctuations in loads and torque are only due to the wake of the upstream surging rotor. In view of these observations, the reported values of the standard deviations for rotor 2 are notable.

Fig. 11 shows the correlation plots of the fluctuations in power and thrust coefficients for the upstream and downstream rotors. The C_P and C_T of rotor 1 are negatively correlated with the coefficients of rotor 2. This means that when rotor 1 is experiencing instantaneous loads/moments higher than its mean, rotor 2 experiences instantaneous values smaller than its mean. More importantly, the correlation between the signals reduces as the surge amplitudes grows. The correlation coefficients of the C_P data decrease from 0.72 to 0.65 and 0.60 when the surge amplitude increases from 1.02 m to 2.04 m and 3.06 m. The correlation coefficients of the C_T data decrease from 0.72 to 0.66 and 0.62 when the surge amplitude increases from 1.02 m to 2.04 m and 3.06 m.

Fig. 12 shows the power spectra of the C_P time-series of the upstream and downstream rotors. The frequency analysis of rotor 1 coefficients shows a clear peak at the surge frequency, i.e. 0.11 Hz, and its multiples. A clear impact of rotor 1 surge motion on the power spectra of rotor 2 at x/D = 3 is also observed with a visible peak at the surge frequency. This is in line with experimental observation by Schliffke et al. [32] where the spectral analysis revealed the footprint of the surge frequency on the velocity measurements at x/D = 4.6, downstream a surging actuator disc. In

addition, due to the surge motion, an increase in the energy content of the spectrum is observed for both rotors against the fixed rotor. The figure shows other peaks at lower frequencies for rotor 2, where such peaks are insignificant for rotor 1. More specifically, a peak at a frequency of 0.01 Hz (and peaks at its multiples) is observed, which corresponds to a harmonics with a period of nearly 11 surge periods. Such low-frequency period is also apparent in the time-series data shown in Fig. 8c–d and 9c-d at time/surge periods of 96.5 and 107.5, as well as the spatiotemporal contours illustrated in Fig. 10. The energy content of these low-frequency peaks is found to grow for higher surge amplitudes. Clarification of the underlying mechanism for the low-frequency peaks requires detailed flow analysis.

4. Wake interactions

In this section, three cases are selected for detailed aerodynamic analysis of wake interactions between floating wind turbines. Two 'surging cases', corresponding to the lowest and highest studied surge amplitudes of 1.02 m (A1 case) and 3.06 m (A3 case), see Sec. 3. In addition to the surging cases, the case where both rotors are fixed is also included as a basis to clarify the impact of the aerodynamic unsteadiness on the wake interactions. This case is referred to as the 'fixed case'.

Fig. 13 illustrates the contour plots of the time-averaged pressure coefficient CoP, dimensionless velocity deficit $\frac{\Delta u_m}{U_\infty}$, defined using Eq. (6), and dimensionless velocity fluctuations, defined as the ratio of the standard deviation of fluctuations of axial velocity u' over the time-averaged axial velocity u_m. U_∞ correspond to free-stream velocity. The presented analysis is based on data corresponding to 15 full surge periods to well-represented statistical data. Note that the term $\frac{u_{std}}{u_m}$ is equivalent to turbulence level generated over the 15 surge periods.
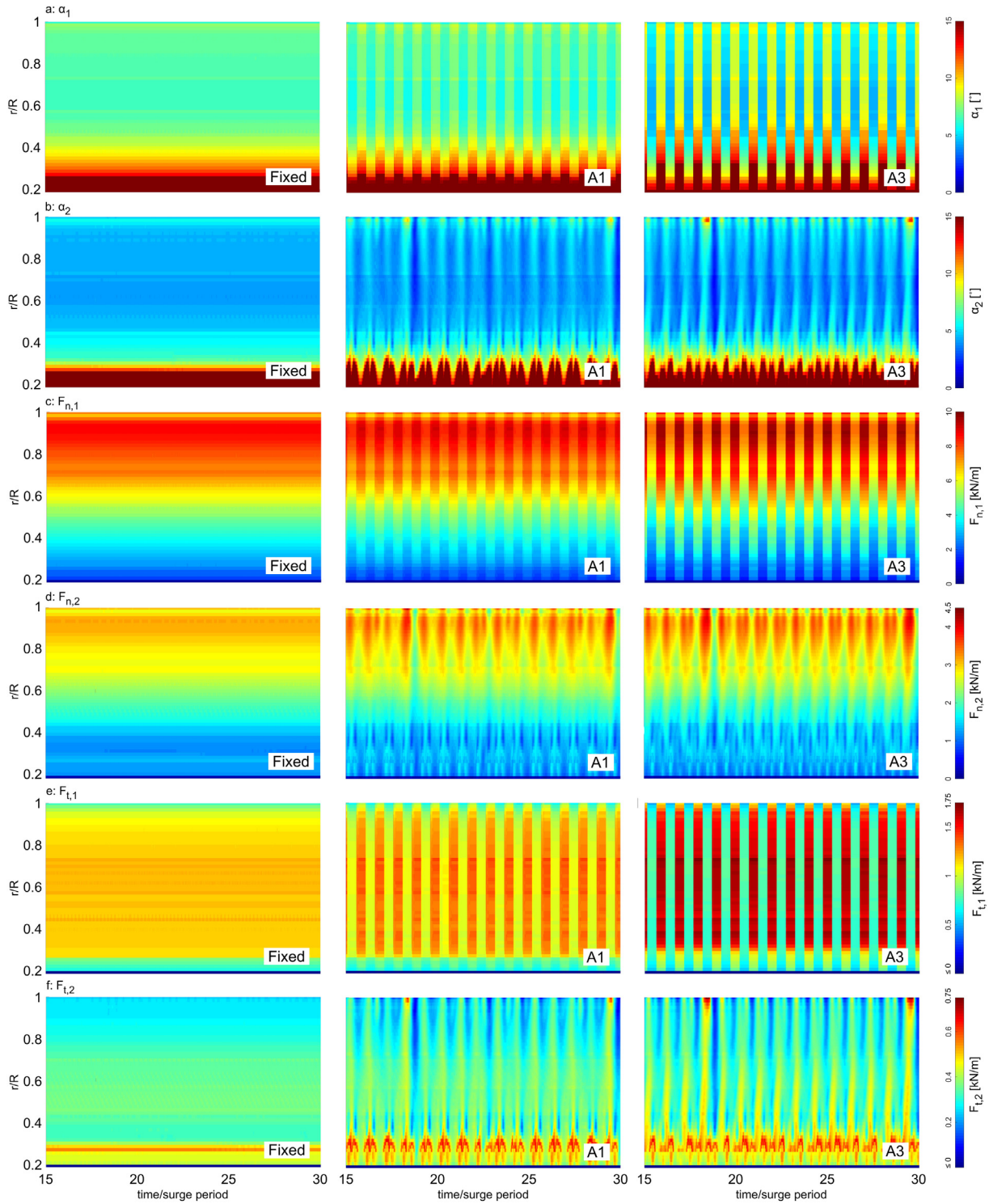
Fig. 10. Spatiotemporal contour plots of angle of attack, tangential and normal loads (per unit span) for the upstream and downstream rotors.

$$\frac{\Delta u_m}{U_\infty} = \frac{U_\infty - u_m}{U_\infty} \tag{6}$$

At first, a comparison is made between the fixed case against A1 case. The comparison reveals that although negligible differences in the time-averaged pressure and velocity field in the wake of rotor 1 are observed, on the contrast, significant differences are evident for rotor 2 due to its interactions with the wake of the upstream

floating rotor. The contour plots of velocity deficit, given in Fig. 13, shows that for A1 case, the magnitude and the streamwise extent of the low velocity region in the wake of rotor 2 are substantially more limited, compared to the fixed case. For the fixed case, as an example, the high velocity deficit region ($\frac{\Delta u_m}{U_\infty} > 0.5$) at inboard rotor section, extends up to 7D downstream (x/D = 10), this is while the corresponding value for A1 case is nearly 4.5D downstream (x/D ≈ 7.5). Fig. 13a also shows that the pressure field re-energizes to

Table 3
Mean and standard deviation (σ) of power and thrust coefficients for both rotors.

|	Case	$A[m]$	$\sigma_T[kN]$	$\overline{C_T}$	σ_{C_T}	$\frac{\sigma_{C_T}[\%]}{\overline{C_T}}$	$\sigma_M[MNm]$	$\overline{C_P}$	σ_{C_P}	$\frac{\sigma_{C_P}[\%]}{\overline{C_P}}$
rotor1	fixed	0.00	0.12	0.7153			0.00	0.5667		
	A1	1.02	26.82	0.7146	0.027	3.8	0.43	0.5672	0.048	8.4
	A2	2.04	52.68	0.7137	0.053	7.4	0.84	0.5701	0.094	16.5
	A3	3.06	78.28	0.7118	0.079	11.1	1.24	0.5737	0.139	24.1
rotor2	fixed	0.00	0.28	0.2742			0.00	0.1611		
	A1	1.02	16.42	0.2743	0.017	6.0	0.20	0.1633	0.022	13.7
	A2	2.04	18.35	0.2730	0.019	6.8	0.23	0.1622	0.026	15.9
	A3	3.06	20.41	0.2766	0.021	7.4	0.26	0.1678	0.029	17.2
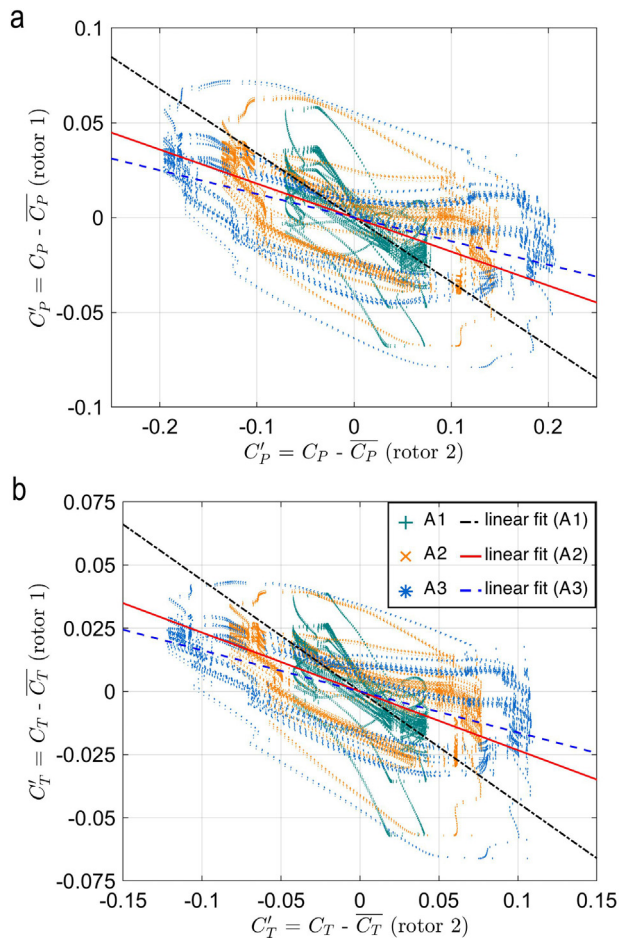
Fig. 11. Correlation plots of the fluctuations in power and thrust coefficients for the upstream and downstream rotors.

Fig. 12. Power spectra of the C_P for both upstream and downstream rotors.

higher values at comparatively earlier streamwise position for A1 case. In addition to the velocity and pressure fields, as shown in Fig. 13c, the floating motion of rotor 1, which results in large oscillations in the aerodynamic loads, is found to create high unsteadiness in terms of velocity fluctuations in the wake of rotor 1. This is then substantially amplified when this unsteady wake approaches rotor 2 and is reflected as a large increase in turbulence level at the incidence of rotor 2 and in its wake.

Regarding the impact of surge amplitude, it is found to slightly amplify the discussed observations due to the floating surge motion. This is more evidently observable in the pressure and velocity fields. For example, by tripling the surge amplitude from 1.02 m (A1) to 3.06 m (A3), the streamwise extent of the high velocity deficit region at inboard rotor section, marginally reduces from x/
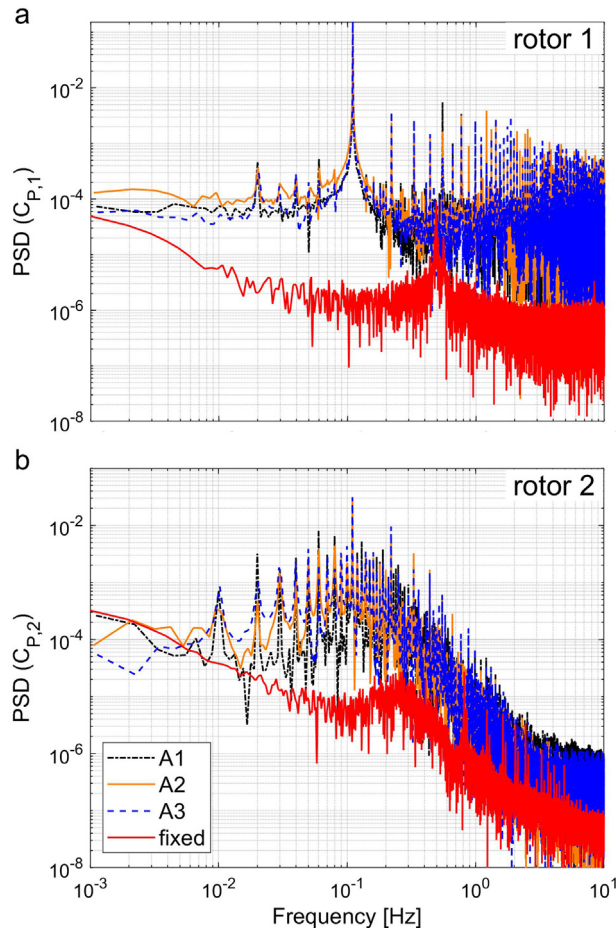
$D \approx 7.5$ to ≈ 7.0. Similar observation can also be made from the pressure field.

To facilitate more quantitative comparison, Figs. 14–15 present the wake recovery, in terms of dimensionless velocity deficit and turbulence level, along the streamwise direction at different lateral heights of y/D = 0.3, 0.4, and 0.5. The time-averaged velocity deficit in the near wake of the surging cases for streamwise positions of x/D ≤ 3, upstream of rotor 2, is hardly different than the fixed case. However, there is significantly higher unsteadiness in the wake of the surging rotor compared to the fixed case at the same streamwise locations, see 15. Because of this higher turbulence level in the approaching flow to rotor 2, the time-averaged velocity deficit for the surging cases downstream of rotor 2 (x/D > 3) are substantially lower than that of the fixed case.

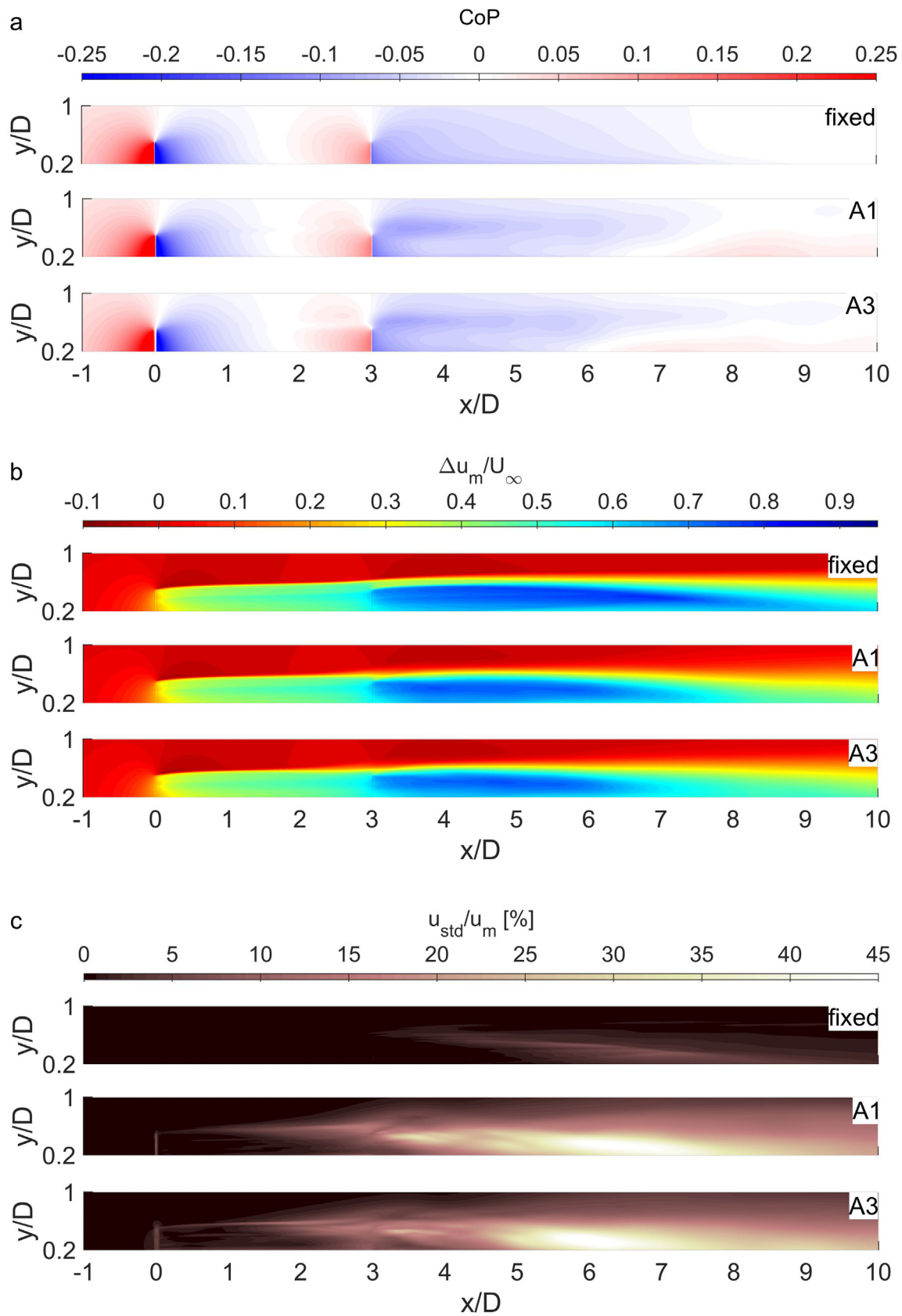**Fig. 13.** Contour plots of time-averaged (over 15 surge periods) pressure coefficient (a), dimensionless velocity deficit (b) and velocity fluctuations (c).
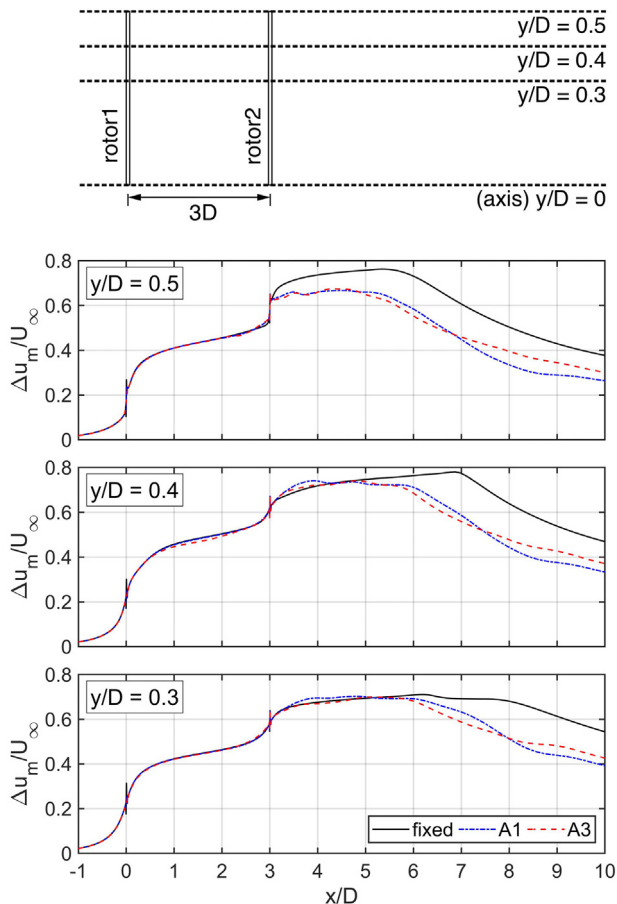
Fig. 14. Wake recovery: dimensionless velocity deficit along streamwise direction.

Fig. 15. Wake recovery: dimensionless velocity fluctuation along streamwise direction.

In addition, the turbulence level is found to grow for higher surge amplitude and for spanwise positions towards the tip. This directly influences the time-averaged velocity deficit downstream of rotor 2 for surging cases. Near the rotor tip at y/D = 0.5, lower velocity deficit for the surging cases is already observed at $x/D > 3$, compared to the fixed case. This difference is observed at x/D ≥ 4.6 and 5.5 at inner sections of y/D = 0.4 and 0.3. The trend is in line with lower turbulence level for smaller y/D.

Another observation is that near the rotor tip at y/D = 0.5, for the fixed case the wake starts to recover (velocity deficit begins to monotonically drop) at x/D ≈ 5.3. At the same height the wake recovery starts earlier at x/D ≈ 5.1 and 4.3 for the surging A1 and A3 cases, respectively. The streamwise onset of the wake recovery is almost consistent with the peak in the turbulence level, from which further downstream the turbulence level is reducing. For the fixed case, the wake recovery onset shifts further downstream to x/D ≈ 6.9 and 7.6 at y/D = 0.4 and 0.3, respectively. The wake recovery onset at y/D = 0.4 and 0.3 for A1 is ≈ 6 and 6.1, respectively, and for case A3 is ≈ 5.8 and 6.1, respectively. The presented analysis, on the one hand, reveals that the unsteadiness due to surging of the upstream rotor results in amplified vertical mixing for the downstream rotor from the rotor top inwards so that the flow at inboard sections begins to recover much earlier than the fixed case. On the other hand, the role of surge amplitude in this process is marginal and higher surge amplitudes will have limited effect.

To further elaborate this, Fig. 16 present the wake recovery, in terms of dimensionless velocity deficit and turbulence level, along the lateral direction at different downstream locations corresponding to x/D = 1.0, 2.0, 4.0, 5.0, 6.0, 7.0, and 8.0. As early as 2D
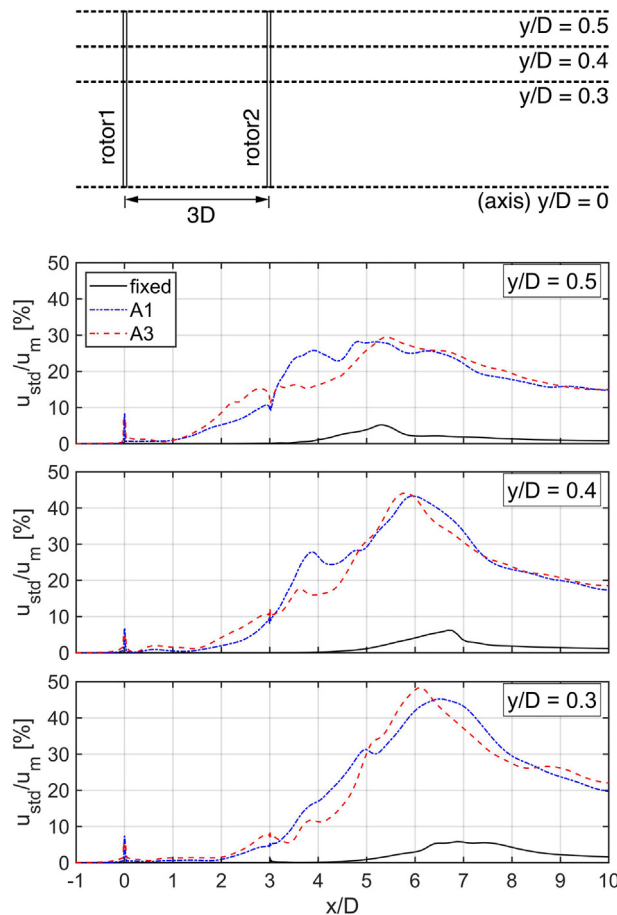
downstream of the surging rotor, flow above the rotor top begins to differ from the fixed case both in terms of time-averaged velocity deficit and flow unsteadiness. This difference grows as the flow approaches rotor 2 and in its wake. As the flow travels downstream at x/D ≥ 4, flow with higher momentum (seen as lower velocity deficit and higher turbulence level) is found to penetrate inward the rotor inboard sections and this mixing process occurs much faster for the surging cases compared to the fixed case. The observed enhanced mixing, which occurs due to the higher unsteadiness caused by the surging of rotor 1, is the responsible mechanism for the faster wake recovery of rotor 2.

This finding proves that wind farm layout design for FOWTs needs to be revisited as potential for more compact spacing of the rotors and therefore, higher wind farm power density exists.

5. Discussion

5.1. Limitations of the study

The outlook to extend this work is focused on improving the modeling approach with respect to the limitations of this work:

Dynamic airfoil data: A first improvement could be to replace the static airfoil data, which is an input to the actuator disc model, with a set of polars for transient pitching airfoils obtained from high-fidelity CFD or experiments, i.e. the dynamic airfoil data. This will make sure that the unsteady aerodynamic effects due to constant variations in the angle of attack is directly influencing the transient lift and drag values and consequently the rotor power performance
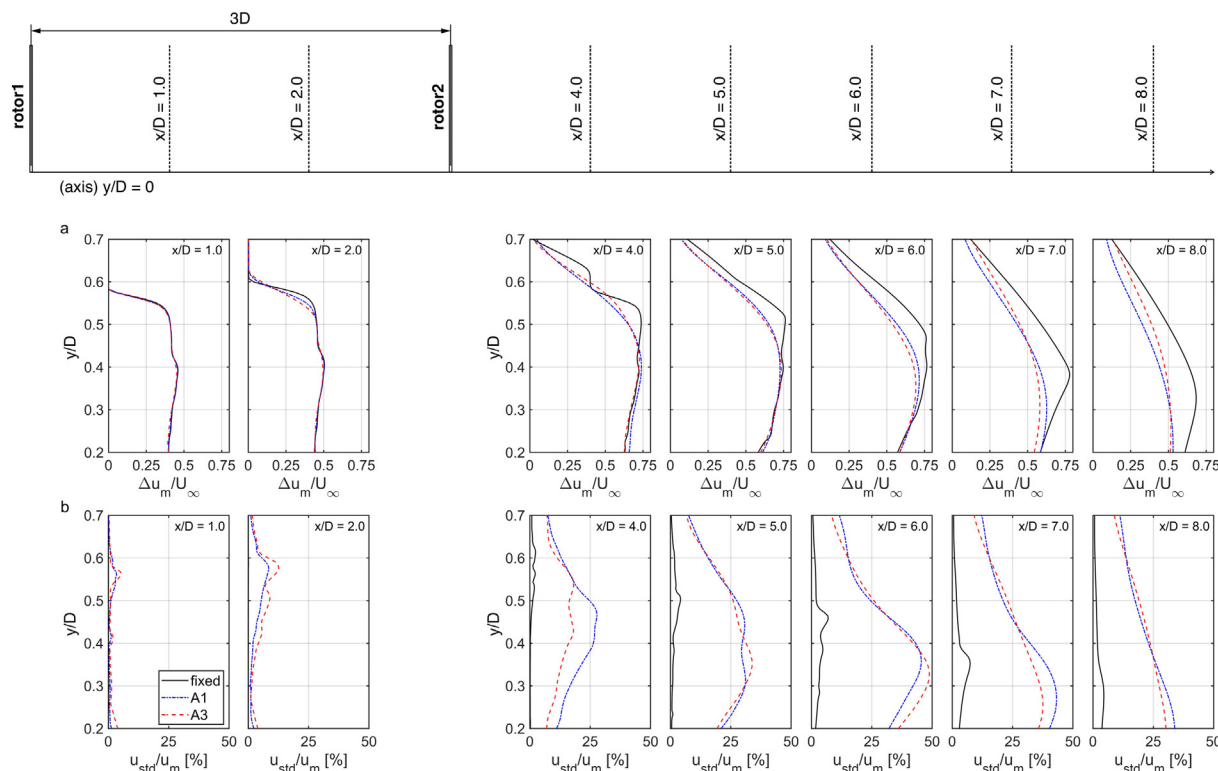
Fig. 16. Wake recovery: dimensionless velocity deficit and fluctuations along lateral direction.

and the wake. It must be noted that preparing such data sets would be challenging as it would require many numerical/experimental simulations. This would be very time-consuming and (computationally) expensive. Apart from this, such data sets need to be developed for all the airfoil sections employed across the span and this further adds to the complexity.

3D modeling: In addition, the axisymmetric modeling can be upgraded to a full 3D modeling at the cost of much higher computational effort. This would enable capturing the three-dimensional phenomena in the wake, such as wake meandering and their dependency on the floating motion. On the other hand, employing the full 3D modeling would allow for investigation of potential cases where the tandem rotors are not fully inline, and (horizontally or vertically) staggered arrangements could also be investigated. This could further allow to explore possibilities to leverage the inherent unsteadiness due to the floating motion towards optimal layout design of floating wind farms. In addition, the 3D modeling would also allow to include other out-of-plane platform motions such as yaw and would make the simulations more realistic by considering 6DoF motion.

Higher fidelity aerodynamic models: Another point of improvement could be to go for higher fidelity aerodynamic models such as actuator line or lifting line at the expense of the higher computational cost. However, we have opted for the simplest rotor modeling approach, which could also be of high interest for the industry. Indeed, future studies using more complex modeling approaches can show whether the additional complexity and computational cost would justify the improvement in the predictions.

More detailed turbulence modeling approach: Furthermore, as flow unsteadiness and turbulence are key role players, the turbulence modeling approach can be upgraded from URANS towards the more complex scale-resolving approaches such as scale-adaptive simulation (SAS) [46], hybrid RANS/LES, or large eddy

simulation (LES). This would provide flow data with a higher level of spatiotemporal resolution, which could shed more light into the underlying physical mechanisms.

Multi-physics modeling of FOWTs: Another potential improvement in the modeling, which is significantly more challenging to be achieved, is to develop a fully coupled aero-hydrodynamic approach to remove the assumption of having the downstream rotor fixed. This would require updating the positioning of the downstream rotor due to the collective aero-hydrodynamic force on the rotor and platform and would require a delicate modeling approach to balance accuracy and computational cost.

5.2. Future perspective on FOWT research

While the current research on FOWTs is focused on elucidating flow complexities associated with an isolated single floating rotor, the present study reveals that complex wake interactions could occur when the scope of research would expand to multiple floating rotors. It is also shown that wind farm layout for FOWTs could be different due to these interactions. More fundamental and extensive understanding on such complexities could not be obtained unless further studies would focus on wake interactions of FOWTs using models of varying fidelity and address the limitations of this study. After all, FOWTs would eventually operate in arrangements and such interactions need to be fully understood before we can leverage the potential of floating wind farms.

6. Conclusions

CFD simulations coupled with an actuator disc model are employed to analyze the wake interactions of floating offshore wind turbines. The case of study is two tandem NREL 5 MW rotors with a small distance of 3 rotor diameters, where the upstream rotor (rotor 1) is surging with different amplitudes and the

downstream rotor (rotor 2) is fixed. For comparison, a case where both rotors are fixed is also included. The analysis focuses on the influence of floating motion on the time-averaged and transient power performance of both rotors and their wake interactions. The main conclusions are as follows:

- The time-averaged power and thrust coefficients (over 100 surge periods) of both upstream and downstream rotors are found to be negligibly affected by the surge motion and the values are insignificantly different than the fixed rotor case. The C_P values of rotor 1 and 2 marginally increase by 1.2% and 4.2% for the highest surge amplitude of 3.06 m.
- The C_P and C_T of rotor 1 are oscillating with a quasi-sinusoidal motion, dominated by the periodic surge motion of the platform. σ_{C_P} of rotor 1 scales up from 8.4% to 24.1%, of the respective mean C_P value. The increase is proportional to the increase in surge amplitude from 1.02 m to 3.06 m.
- In contrast to rotor 1, the transient C_P and C_T time-series of rotor 2 are quite complex signals with several harmonics involved, other than only the main harmonics of the surge motion. A signature low-frequency period is observed in the signals of rotor 2, which is absent in the corresponding signals of rotor 1. The overall trend of the oscillating signals of rotor 2 is almost invariant to the surge amplitude. The σ_{C_P} of rotor 2 grows from 13.7% to 17.2%, of the respective mean C_P values, when surge amplitude increases from 1.02 m to 3.06 m. Thus, doubling and tripling the surge amplitude increases σ_{C_P} by only 15.7% and 29.1%.
- The transient C_P and C_T values of the upstream surging rotor are negatively correlated with the same coefficients of the downstream rotor.

- The time-averaged velocity deficit in the wake of the upstream surging rotor is comparable to a fixed rotor. However, the wake flow includes significantly higher unsteadiness. This has noticeable influences on the downstream rotor, where both the time-averaged velocity field and the turbulence level are largely different than the fixed rotor case. Vertical mixing with high momentum flow above the rotor is largely amplified due to the unsteadiness caused by the surging motion of rotor 1 and this results in earlier penetration of high energy flow inwards the rotor wake and consequently faster wake recovery. This important potential is the promising point, which reveals the fact that the unsteadiness due to floating can be leveraged to design more compact wind farms with higher power density.

Declaration of competing interest

The authors declare that they have no known competing financial interests or personal relationships that could have appeared to influence the work reported in this paper.

Acknowledgments

Appendix A. Literature review table

Table A.1
Recent publications on aerodynamics of floating offshore wind turbine with surge motion. The table excludes model validation and cross-code comparisons. Note: TLP - Tension-leg platform; Num - Numerical; Exp - Experimental; CFD-AD - CFD using an Actuator Disc; CFD-AL - CFD using an Actuator Line; FVWM - Free Vortex Wake Method; NVLM - Non-linear Vortex Lattice Method; VPM - Vortex Particle Method; CRAFT - Coupled Response Analysis of Floating wind Turbine; BEM - Blade Element Momentum.

Publication	Year	Publication type	Foundation type	Rotor rating	Method	Focus of study
Rezaeiha and Micallef [40]	2020	Journal	N/A	5 MW (NREL)	Num (CFD-AD)	power performance study for two tandem rotors
Johlas et al. [50]	2020	Journal	spar buoy, semi-submersible	5 MW (NREL)	Num (CFD-AL)	wake study
Dong and Viré [51]	2020	Journal	spar buoy, barge, TLP	5 MW (NREL)	Num (FAST)	vortex ring state identification
Schliffke et al. [32]	2020	Journal	N/A	Porous disc	Exp	wake study and spectral analysis
Li et al. [52]	2020	Journal	Submersible	5 MW (OC4)	Num (FAST)	effects of yaw error on platform motions and performance
Kyle et al. [31]	2020	Journal	barge	5 MW (NREL)	Num (CFD)	propeller and vortex ring states identification
Kopperstad et al. [30]	2020	Journal	spar buoy, barge	Model porous disc	Num (CFD-AD)	near wake study
Wang et al. [5]	2019	Conference proceedings	TLP	N/A	Num (BEM)	dynamic response analysis
Bezzina et al. [47]	2019	Conference proceedings	TLP	Model scale rotor, 10 W	Num (CFD-AD)	power performance study
Lee and Lee [53]	2019	Journal	Prescribed motions	5 MW (NREL)	Num (NVLM and VPM)	wake study
Shen et al. [18]	2018	Journal	Prescribed motions	5 MW (NREL)	Num (FVWM)	wake study and power performance study
Tran and Kim [29]	2016	Journal	Prescribed motions	5 MW (NREL)	Num (CFD)	power performance study
Shen et al. [54]	2016	Journal	TLP	5 MW (NREL)	Num (CRAFT)	dynamic response analysis
Farrugia et al. [26]	2016	Journal	TLP	5 MW (NREL)	Num (FVWM)	power performance study
Tran et al. [28]	2015	Journal	Prescribed motions	5 MW (NREL)	Num (CFD)	power performance study
Sant et al. [21]	2015	Journal	TLP	Model scale rotor, 10 W	Exp	power performance study
Micallef and Sant [22]	2015	Journal	TLP	5 MW (NREL)	Num (CFD-AD)	power performance study
Sebastian and Lackner [55]	2013	Journal	monopile, barge, spar-buoy and TLP	5 MW (NREL)	Num (FAST)	near wake study
Sebastian and Lackner [14]	2012	Journal	monopile, barge, spar buoy, and TLP	5 MW (NREL)	Num (FVWM)	power performance study at different tip speed ratios
Jonkman and Matha [56]	2011	Journal	spar buoy, barge, TLP	5 MW (NREL)	Num (FAST)	dynamic response analysis for different foundations
Robertson et al. [57]	2011	Conference proceedings	Spar buoy	5 MW (NREL)	Num (FAST)	power performance study
Matha [58]	2010	Technical report	TLP	5 MW (NREL)	Num (FAST)	loads and stability analysis for ultimate and fatigue loads

References

[1] N. Bento, M. Fontes, Emergence of floating offshore wind energy: technology and industry, Renew. Sustain. Energy Rev. 99 (2019) 66–82, https://doi.org/10.1016/j.rser.2018.09.035. URL, http://www.sciencedirect.com/science/article/pii/S1364032118306841.

[2] J. Bosch, I. Staffell, A.D. Hawkes, Global levelised cost of electricity from offshore wind, Energy 189 (2019) 116357, https://doi.org/10.1016/j.energy.2019.116357. URL, http://www.sciencedirect.com/science/article/pii/S0360544219320523.

[3] M. Kausche, F. Adam, F. Dahlhaus, J. Großmann, Floating offshore wind - economic and ecological challenges of a TLP solution, Renew. Energy 126 (2018) 270–280, https://doi.org/10.1016/j.renene.2018.03.058. URL, http://www.sciencedirect.com/science/article/pii/S0960148118303690.

[4] A. Rezaeiha, R. Pereira, M. Kotsonis, Fluctuations of Angle of Attack and Lift Coefficient and the Resultant Fatigue Loads for a Large Horizontal Axis Wind Turbine, Renewable Energy, 2017, https://doi.org/10.1016/j.renene.2017.07.101.

[5] T. Wang, H. Jin, X. Wu, Coupled dynamic analysis of a tension leg platform floating offshore wind turbine, J. Offshore Mech. Arctic Eng. 142 (2019), https://doi.org/10.1115/1.4044075.

[6] Y. Liu, Q. Xiao, A. Incecik, C. Peyrard, D. Wan, Establishing a fully coupled CFD analysis tool for floating offshore wind turbines, Renew. Energy 112 (2017) 280–301, https://doi.org/10.1016/j.renene.2017.04.052. URL, http://www.sciencedirect.com/science/article/pii/S0960148117303609.

[7] Y.P. Chodnekar, S. Mandal, K. Balakrishna Rao, Hydrodynamic analysis of floating offshore wind turbine, Procedia Eng. 116 (2015) 4–11, https://doi.org/10.1016/j.proeng.2015.08.258.

[8] P. Trubat, C. Molins, X. Gironella, Wave hydrodynamic forces over mooring lines on floating offshore wind turbines, Ocean Eng. 195 (2020) 106730, https://doi.org/10.1016/j.oceaneng.2019.106730.

[9] M.L.B. Jr, FAST User ' S Guide Updated August 2005 FAST User ' S Guide Updated August 2005, Contract, 2005.

[10] L. Roald, J. Jonkman, A. Robertson, N. Chokani, The effect of second-order hydrodynamics on floating offshore wind turbines, Energy Procedia 35 (2013) 253–264, https://doi.org/10.1016/j.egypro.2013.07.178.

[11] G.K.Y. Chan, P.D. Sclavounos, J. Jonkman, G. Hayman, Computation of nonlinear hydrodynamic loads on floating wind turbines using fluid-impulse theory, in: Proceedings of the International Conference on Offshore Mechanics and Arctic Engineering - OMAE 9, 2015, https://doi.org/10.1115/OMAE2015-41053.

[12] H. Shin, P.T. Dam, K.J. Jung, J. Song, C. Rim, T. Chung, Model test of new floating offshore wind turbine platforms, Int. J. Nav. Architect. Ocean Eng. 5 (2013) 199–209, https://doi.org/10.2478/ijnaoe-2013-0127. URL.

[13] T. Sebastian, M. Lackner, Offshore floating wind turbines - an aerodynamic perspective, in: 49th AIAA Aerospace Sciences Meeting Including the New Horizons Forum and Aerospace Exposition, 2011, https://doi.org/10.2514/6.2011-720. URL, https://arc.aiaa.org/doi/abs/10.2514/6.2011-720.

[14] T. Sebastian, M. Lackner, Analysis of the induction andwake evolution of an offshore floating wind turbine, Energies 5 (2012) 968–1000, https://doi.org/10.3390/en5040968.

[15] D. Micallef, A. Rezaeiha, Floating Offshore Wind Turbine Aerodynamics: Trends and Future Challenges submitted for publication, 2020.

[16] Y. Fang, L. Duan, Z. Han, Y. Zhao, H. Yang, Numerical analysis of aerodynamic performance of a floating offshore wind turbine under pitch motion, Energy 192 (2020) 116621, https://doi.org/10.1016/j.energy.2019.116621. doi:10.1016/j.energy.2019.116621. URL.

[17] S. Fu, Y. Jin, Y. Zheng, L.P. Chamorro, Wake and power fluctuations of a model wind turbine subjected to pitch and roll oscillations, Appl. Energy 253 (2019) 113605, https://doi.org/10.1016/j.apenergy.2019.113605. URL, http://www.sciencedirect.com/science/article/pii/S0306261919312796.

[18] X. Shen, J. Chen, P. Hu, X. Zhu, Z. Du, Study of the unsteady aerodynamics of floating wind turbines, Energy 145 (2018) 793–809, https://doi.org/10.1016/j.energy.2017.12.100. URL, http://www.sciencedirect.com/science/article/pii/S0360544217321436.

[19] V. Leble, G. Barakos, 10-MW wind turbine performance under pitching and yawing motion, J. Sol. Energy Eng. 139 (2017).

[20] B. Wen, X. Dong, X. Tian, Z. Peng, W. Zhang, K. Wei, The power performance of an offshore floating wind turbine in platform pitching motion, Energy 154 (2018) 508–521, https://doi.org/10.1016/j.energy.2018.04.140. URL, http://www.sciencedirect.com/science/article/pii/S0360544218307564.

[21] T. Sant, D. Bonnici, R. Farrugia, D. Micallef, Measurements and modelling of the power performance of a model floating wind turbine under controlled conditions, Wind Energy 18 (2015) 811–834, https://doi.org/10.1002/we.1730.

[22] D. Micallef, T. Sant, Loading effects on floating offshore horizontal axis wind turbines in surge motion, Renew. Energy 83 (2015) 737–748, https://doi.org/10.1016/j.renene.2015.05.016. URL, http://linkinghub.elsevier.com/retrieve/pii/S0960148115003936.

[23] M. Jeon, S. Lee, S. Lee, Unsteady aerodynamics of offshore floating wind turbines in platform pitching motion using vortex lattice method, Renew. Energy 65 (2014) 207–212, https://doi.org/10.1016/j.renene.2013.09.009. URL, http://www.sciencedirect.com/science/article/pii/S096014811300476X.

[24] L. Lin, K. Wang, D. Vassalos, Detecting wake performance of floating offshore wind turbine, Ocean Eng. 156 (2018) 263–276.

[25] S. Mancini, K. Boorsma, M. Caboni, M. Cormier, T. Lutz, P. Schito, A. Zasso, Characterization of the Unsteady Aerodynamic Response of a Floating Offshore Wind Turbine, 2020, pp. 1–26.

[26] R. Farrugia, T. Sant, D. Micallef, A study on the aerodynamics of a floating wind turbine rotor, Renew. Energy 86 (2016) 770–784, https://doi.org/10.1016/j.renene.2015.08.063. URL, http://linkinghub.elsevier.com/retrieve/pii/S0960148115302639.

[27] J.B. de Vaal, M.O.L. Hansen, T. Moan, Effect of wind turbine surge motion on rotor thrust and induced velocity, Wind Energy 17 (2014) 105–121, https://doi.org/10.1002/we.1562.

[28] T. Tran, D. Kim, B. Nguyen, Aerodynamic interference effect of huge wind turbine blades with periodic surge motions using overset grid-based computational fluid dynamics approach, J. Sol. Energy Eng. 137 (2015).

[29] T.T. Tran, D.-H. Kim, A CFD study into the influence of unsteady aerodynamic interference on wind turbine surge motion, Renew. Energy 90 (2016) 204–228.

[30] K.M. Kopperstad, R. Kumar, K. Shoele, Aerodynamic Characterization of Barge and Spar Type Floating Offshore Wind Turbines at Different Sea States, Wind Energy, 2020, pp. 1–26, https://doi.org/10.1002/we.2547.

[31] R. Kyle, Y.C. Lee, W.G. Früh, Propeller and vortex ring state for floating offshore wind turbines during surge, Renew. Energy 155 (2020) 645–657, https://doi.org/10.1016/j.renene.2020.03.105. URL.

[32] B. Schliffke, S. Aubrun, B. Conan, Wind Tunnel Study of a " Floating " Wind Turbine ' S Wake in an Atmospheric Boundary Layer with Imposed Characteristic Surge Motion Wind Tunnel Study of a " Floating " Wind Turbine ' S Wake in an Atmospheric Boundary Layer with Imposed Characteristic Surg, 2020, https://doi.org/10.1088/1742-6596/1618/6/062015.

[33] N. Troldborg, Actuator Line Modeling of Wind Turbine Wakes, Phd, Technical University of Denmark, 2009. Copenhagen.

[34] H. Sarlak, C. Meneveau, J.N. Sørensen, Role of subgrid-scale modeling in large eddy simulation of wind turbine wake interactions, Renew. Energy 77 (2015) 386–399, https://doi.org/10.1016/j.renene.2014.12.036. URL.

[35] S. Sahebzadeh, A. Rezaeiha, H. Montazeri, Towards optimal layout design of vertical-axis wind-turbine farms: double rotor arrangements, Energy Convers. Manag. 226 (2020) 113527.

[36] S. Zanforlin, T. Nishino, Fluid dynamic mechanisms of enhanced power generation by closely spaced vertical axis wind turbines, Renew. Energy 99 (2016) 1213–1226.

[37] B. Hand, A. Cashman, Conceptual design of a large-scale floating offshore vertical axis wind turbine, Energy Procedia 142 (2017) 83–88.

[38] A. Rezaeiha, M. Tirandaz, Effect of airfoil shape on power performance of vertical axis wind turbines in dynamic stall: symmetric airfoils, Renew. Energy 173 (2021) 422–441.

[39] S. Rockel, E. Camp, J. Schmidt, J. Peinke, R.B. Cal, M. Hölling, Experimental Study on Influence of Pitch Motion on the Wake of a Floating Wind Turbine Model, vol. 7, 2014, https://doi.org/10.3390/en7041954.

[40] A. Rezaeiha, D. Micallef, CFD simulation of two tandem floating offshore wind turbines in surge motion, J. Phys. Conf. 1618 (2020), 052066, https://doi.org/10.1088/1742-6596/1618/5/052066. URL, https://iopscience.iop.org/article/10.1088/1742-6596/1618/5/052066.

[41] J. Jonkman, S. Butterfield, W. Musial, G. Scott, Definition of a 5-MW Reference Wind Turbine for Offshore System Development, Report, NREL, 2009.

[42] ANSYS, ANSYS® Fluent Theory Guide, Release 16.1, ANSYS, Inc., Report, 2015.

[43] A. Rezaeiha, I. Kalkman, B. Blocken, Cfd simulation of a vertical axis wind turbine operating at a moderate tip speed ratio: guidelines for minimum domain size and azimuthal increment, Renew. Energy 107 (2017) 373–385.

[44] A. Rezaeiha, H. Montazeri, B. Blocken, Towards accurate cfd simulations of vertical axis wind turbines at different tip speed ratios and solidities: guidelines for azimuthal increment, domain size and convergence, Energy Convers. Manag. 156 (2018) 301–316.

[45] A. Rezaeiha, H. Montazeri, B. Blocken, On the accuracy of turbulence models for cfd simulations of vertical axis wind turbines, Energy 180 (2019) 838–857.

[46] A. Rezaeiha, H. Montazeri, B. Blocken, Cfd analysis of dynamic stall on vertical axis wind turbines using scale-adaptive simulation (sas): comparison against urans and hybrid rans/les, Energy Convers. Manag. 196 (2019) 1282–1298.

[47] R. Bezzina, T. Sant, D. Micallef, Modelling the aerodynamics of a floating wind turbine model using a CFD-based actuator, Disc Method (2019) 1–12.

[48] H. Glauert, Aerodynamic Theory, Dover, New York, 1963, pp. 169–360.

[49] M.L.B. Jr, FAST User ' S Guide Updated August 2005 FAST User ' S Guide Updated August 2005, Contract, 2005.

[50] H.M. Johlas, L.A. Martínez-Tossas, M.A. Lackner, D.P. Schmidt, M.J. Churchfield, Large eddy simulations of offshore wind turbine wakes for two floating platform types, J. Phys. Conf. 1452 (2020), https://doi.org/10.1088/1742-6596/1452/1/012034.

[51] J. Dong, A. Viré, Predicting the occurrence of the vortex ring state for floating offshore wind turbines, J. Phys. Conf. 1618 (2020), 052044, https://doi.org/10.1088/1742-6596/1618/5/052044. URL, https://iopscience.iop.org/article/10.1088/1742-6596/1618/5/052044.

[52] X. Li, C. Zhu, Z. Fan, X. Chen, J. Tan, Effects of the yaw error and the wind-wave misalignment on the dynamic characteristics of the floating offshore wind turbine, Ocean Eng. 199 (2020) 106960, https://doi.org/10.1016/j.oceaneng.2020.106960. URL.

[53] H. Lee, D.J. Lee, Effects of platform motions on aerodynamic performance and unsteady wake evolution of a floating offshore wind turbine, Renew. Energy

143 (2019) 9—23, https://doi.org/10.1016/j.renene.2019.04.134. URL.

[54] M. Shen, Z. Hu, G. Liu, Dynamic response and viscous effect analysis of a TLP-type floating wind turbine using a coupled aero-hydro-mooring dynamic code, Renew. Energy 99 (2016) 800—812, https://doi.org/10.1016/j.renene.2016.07.058. URL, http://www.sciencedirect.com/science/article/pii/S0960148116306735.

[55] T. Sebastian, M.A. Lackner, Characterization of the unsteady aerodynamics of offshore floating wind turbines, Wind Energy 16 (2013) 339—352, https://doi.org/10.1002/we.545. URL, https://onlinelibrary.wiley.com/doi/abs/10.1002/we.545.

[56] J.M. Jonkman, D. Matha, Dynamics of offshore floating wind turbines—analysis of three concepts, Wind Energy 14 (2011) 557—569, https://doi.org/10.1002/we.442. URL, https://onlinelibrary.wiley.com/doi/abs/10.1002/we.442.

[57] A.N. Robertson, J.M. Jonkman, Others, Loads analysis of several offshore floating wind turbine concepts, in: The Twenty-First International Offshore and Polar Engineering Conference, International Society of Offshore and Polar Engineers, 2011.

[58] D. Matha, Model Development and Loads Analysis of an Offshore Wind Turbine on a Tension Leg Platform with a Comparison to Other Floating Turbine Concepts: April 2009, Technical Report, National Renewable Energy Lab.(-NREL), Golden, CO (United States), 2010.